

Influence of toroidal magnetic field in multi-accreting tori

D. Pugliese,^{1★} G. Montani,^{2,3}

¹*Institute of Physics, and Research Centre of Theoretical Physics and Astrophysics,
Faculty of Philosophy SIGMA Science, Silesian University in Opava,*

Bezručovo náměstí 13, CZ-74601 Opava, Czech Republic

²*ENEA- R.C. Frascati, UTFUS-MAG, Via Enrico Fermi 45, Frascati, Roma 00044, Italy*

³*Physics Department, “Sapienza” University of Rome, P.le Aldo Moro 5, Roma 00185, Italy*

Accepted XXX. Received YYY; in original form ZZZ

ABSTRACT

We analyzed the effects of a toroidal magnetic field in the formation of several magnetized accretion tori, dubbed as ringed accretion disks (**RADs**), orbiting around one central Kerr supermassive Black Hole (**SMBH**) in **AGNs**, where both corotating and counterrotating disks are considered. Constraints on tori formation and emergence of **RADs** instabilities, accretion onto the central attractor and tori collision emergence, are investigated. The results of this analysis show that the role of the central **BH** spin-mass ratio, the magnetic field and the relative fluid rotation and tori rotation with respect the central **BH**, are crucial elements in determining the accretion tori features, providing ultimately evidence of a strict correlation between **SMBH** spin, fluid rotation and magnetic fields in **RADs** formation and evolution. More specifically we proved that magnetic field and disks rotation are in fact strongly constrained, as tori formation and evolution in **RADs** depend on the toroidal magnetic fields parameters. Eventually this analysis identifies specific classes of tori, for restrict ranges of magnetic field parameter, that can be observed around some specific **SMBHs** identified by their dimensionless spin.

Key words: Black Hole physics–Accretion disks–accretion–magneto-hydrodynamics

1 INTRODUCTION

Magnetic fields are ubiquitous in the Universe, playing a relevant role in the High Energy Astrophysics, and being involved in a broad variety of precesses in several environments, from the early Universe, to solar corona and interstellar medium, or in the Galaxy and galaxy clusters-formation processes, in Pulsars and Magnetars. In many of these situations however the exact role and the origin of the magnetic fields are still to the sorted in a comprehensive picture—see for example (Ryu et al. 2012; Siegel et al. 2013; Colgate et al. 2001; Grasso & Rubinstein 2001; Balbus 2011; Balbus & Hawley 1998). The magnetic field presence in the galactic Black Hole (**BH**) accretion disk environments is a special and intriguing topic. The scenario envisaged by the special situation of **BH** accretion, disk formation, with a conjectured accretion-jet correlation is extremely complex. These issues are in fact still very much debated as often correlated with several problematic inherent the most profound aspects of the **BH** physics. In this article we explore the toroidal magnetic fields influence in the accretion tori formation, their configurations espe-

cially in the emergence of the accretion phase. More specifically, the analysis focuses on the magnetized tori orbiting super-massive Kerr Black Hole (**SMBH**) in galactic nuclei (**AGNs**). An accretion disk is essentially regulated by the balance of different factors as the gravitational, centrifugal and magnetic components. In this work we consider clusters of toroidal (thick disk) configurations centered on a single Kerr **BH**, and prescribed by barotropic models, for which the time-scale of the dynamical processes τ_{dyn} (regulated by the gravitational and inertial forces) is much lower than the time-scale of the thermal ones τ_{therm} (heating, cooling processes and radiation), that is lower than the time-scale of the viscous processes τ_v , or $\tau_{dyn} \ll \tau_{therm} \ll \tau_v$. Consequently the effects of strong gravitational fields are generally dominant with respect to the dissipative ones and predominant to determine the systems unstable phases (Abramowicz & Fragile 2013; Pugliese & Montani 2015). Each torus is then part of the coplanar axis-symmetrical structured toroidal disks, orbiting in the equatorial plane of a single central Kerr **BH**, so called ringed accretion disks (**RADs**), introduced in Pugliese & Montani (2015) and detailed in (Pugliese & Stuchlik 2015, 2016a, 2017a,c, 2018). The **RADs** model follows the possibility that more accretion orbiting configurations can form around very compact

★ E-mail: d.pugliese.physics@gmail.com

objects in the special environment of the **AGNs-BHs** and Quasars. Arising from different **BHs** accretion periods and from the host Galaxy life, such configurations can report, in their characteristics, traces of the different periods during several accretion regimes occurred in the lifetime of non-isolated Kerr **BHs** (Alig et al. 2013; Blanchard et al. 2017; Pugliese&Stuchlik 2018; Nixon et al. 2012). During the evolution of **BHs** in these environments both corotating and counterrotating accretion stages are mixed during various accretion periods of the attractor life (Lovelace&Chou 1996; Carmona-Loaiza et al. 2015; Dyda et al. 2015; Volonteri et al. 2003), thus **RADs** tori may be even misaligned (Aly et al. 2015).

From the observational viewpoint, this complex scenario for the lifetime of a **BH**-accretion disks system, opening eventually a new field of investigation in Astrophysics, implies a rich and diversified set of phenomena which may be associated with **RADs**, reinterpreting the observations analyzed so far in the single-torus framework, in a new interpretive frame represented by the possibility of a multi-tori system. Instabilities of such configurations, we expect, may reveal of crucial significance for the High Energy Astrophysics related especially to accretion onto supermassive **BHs**, and the extremely energetic phenomena occurring in Quasars and **AGNs** that could be observable by the planned X-ray observatory **ATHENA**¹. These configurations can be directly linked to the current models featuring the obscuration of galactic Black Hole X-ray emission. The radially oscillating tori of the couple could be related to the high-frequency quasi periodic oscillations (**QPOs**) observed in non-thermal X-ray emission from compact objects, keeping fingerprint of the discrete radial profile of the couple structure. Moreover, relatively indistinct excesses of the relativistically broadened emission-line components were predicted, arising in a well-confined radial distance in the accretion structure originating by a series of episodic accretion events (Sochora et al. 2011; Karas&Sochora 2010; Schee&Stuchlik 2009, 2013).

Here the **RADs** framework has been used to investigate the influence of the magnetic field also in the formation of the single torus, as a limiting case of the **RADs** and hence in the formation of the multiple case too, comparing results of this study with the situation in absence of the magnetic contribution. Differences between these two cases are particularly evident in the unstable phases due to the tori collision and the accretion. We shall focus on the identification of a possible link between the **RAD** formation and features, the **BH** spin and the relative rotation of the fluids in the **RAD**, looking for a correlation between two or more of these elements and the presence of a toroidal magnetic field, especially on emergencies of the instability phases. Particularly we analyze the situation for a *dual-accretion* phase when two tori are both accreting onto Kerr attractors of a special class, defined through the **BH** dimensionless spin and determined by a special relation between the tori relative rotation. This special context reveals an interesting scenario in the coupling between magnetic field effects and the fluid rotation. The choice of a purely azimuthal (toroidal) magnetic field is particularly adapted to the disks symmetries considered here and largely adopted as initial setup for numerical simu-

lations in several general relativistic magnetohydrodynamic (**GRMHD**) models sharing similar symmetries to the **RAD** considered here (Porth et al. 2017). From the methodological viewpoint, the magnetic field contribution has been then considered as part of the exact general relativity effective potential functions for both the fluid and **RADs**. Finally, we used the exact analytical magnetic field solution widely used and known as the Komissarov solution (Komissarov 2006) – and also (Abramowicz&Fragile 2013; Porth et al. 2017; Pugliese&Montani 2013; Adamek&Stuchlik 2013; Hamersky&Karas 2013; Karas et al. 2014; Cremaschini&Stuchlik 2013; Slany et al. 2013; Kovar et al. 2011; Fragile&Sadowski 2017; Gimeno-Soler&Font 2017) for applications in the context of accretion disks.

The structure of this article is as follows: In Section 2 we introduce the case of perfect fluid tori orbiting a central Kerr **BH**, and we set up the model for magnetized torus, discussing the main quantities and notation used throughout this work. Section 3 contains the main results of our analysis, dealing with the magnetized ringed accretion disk (**RAD**), by considering first the limiting case of non-magnetized **RAD** constituted by a couple of tori orbiting a central Kerr **BH**, and then we concentrate our attention on the situation where a toroidal magnetic field is for each component of the **RAD** system. This section closes with subsection 3.1, where some further considerations on the parameter choice follow and, by considering an extended range of variation for the magnetic field parameter, we discuss a very special class of **RADs** tori. In Section 4 we add some further notes on the **RAD** instabilities considering also the phenomenological implications and the influence of the toroidal magnetic field in the system stability. Section 5 traces the conclusions of our investigation and we discuss our results and observational consequences.

2 MAGNETIZED TORI IN THE KERR SPACETIME

We consider toroidal perfect fluids orbiting in the Kerr spacetime background with metric tensor

$$ds^2 = -dt^2 + \frac{\rho^2}{\Delta} dr^2 + \rho^2 d\theta^2 + (r^2 + a^2) \sin^2 \theta d\phi^2 + \frac{2M}{\rho^2} r (dt - a \sin^2 \theta d\phi)^2, \quad (1)$$

in Boyer-Lindquist (BL) coordinates $\{t, r, \theta, \phi\}$. Here M is a mass parameter and the specific angular momentum is given as $a = J/M$, where J is the total angular momentum of the gravitational source and $\rho^2 \equiv r^2 + a^2 \cos^2 \theta$, $\Delta \equiv r^2 - 2Mr + a^2$, in the following it will be also convenient to introduce the quantity $\sigma \equiv \sin \theta$. We will consider the Kerr Black Hole (**BH**) case defined by $a \in]0, M[$, the extreme Black Hole source $a = M$, and the non-rotating limiting case $a = 0$, which is the Schwarzschild static metric. The horizons $r_- < r_+$ and the static limit r_ϵ^+ are respectively

$$r_\pm \equiv M \pm \sqrt{M^2 - a^2}; \quad r_\epsilon^+ \equiv M + \sqrt{M^2 - a^2 \cos^2 \theta}, \quad (2)$$

it is $r_+ < r_\epsilon^+$ on the plane $\theta \neq 0$ and it is $r_\epsilon^+ = 2M$ on the equatorial plane $\theta = \pi/2$. In the region $r \in]r_+, r_\epsilon^+[$ (ergoregion) it is $g_{tt} > 0$ and t -Boyer-Lindquist coordinate becomes

¹ <http://the-athena-x-ray-observatory.eu/>

spacelike. In this work we investigate toroidal configurations of a perfect magnetized and non magnetized fluids orbiting a Kerr attractor (Pugliese&Montani 2015; Abramowicz&Fragile 2013; Pugliese&Montani 2013; Pugliese et al. 2013). Metric is independent of ϕ and t , as consequence of this the covariant components p_ϕ and p_t of a particle four-momentum are conserved along its geodesic. Therefore, quantities²

$$E \equiv -g_{ab}\xi_t^a p^b, \quad L \equiv g_{ab}\xi_\phi^a p^b, \quad (3)$$

are constants of motion, where $\xi_t = \partial_t$ is the Killing field representing the stationarity of the Kerr geometry and $\xi_\phi = \partial_\phi$ is the rotational Killing field, the vector ξ_t is spacelike in the ergoregion. In general, we may interpret E , for timelike geodesics, as representing the total energy of the test particle coming from radial infinity, as measured by a static observer at infinity, and L as the angular momentum of the particle. Furthermore, Kerr metric 1 is invariant under the application of any two different transformations: $x^a \rightarrow -x^a$ as one of the coordinates (t, ϕ) or the metric parameter a , and the circular geodesic motion is invariant under the mutual transformation of the parameters $(a, L) \rightarrow (-a, -L)$. A consequence of this we can limit the analysis of test particle circular motion to the case of positive values of a , for corotating ($L > 0$) and counterrotating ($L < 0$) orbits. Some notable radii regulate the particle dynamics, namely the *marginally circular orbit* for timelike particles r_γ^\pm , the *marginally bounded orbit* is r_{mbo}^\pm , and the *marginally stable circular orbit* is r_{mso}^\pm with angular momentum and energy ($E_\pm, \mp L_\pm$) respectively, where (\pm) is for counterrotating or corotating orbits with respect to the attractor (Pugliese et al. 2011; Pugliese&Quevedo 2015; Pugliese et al. 2013). In the case a non-magnetized tori we may consider a one-specie particle perfect fluid (simple fluid), where

$$T_{ab} = (\varrho + p)u_a u_b + p g_{ab}, \quad (4)$$

is the fluid energy momentum tensor, ϱ and p are the total energy density and pressure, respectively, as measured by an observer moving with the fluid. For the symmetries of the problem, we always assume $\partial_t \mathbf{Q} = 0$ and $\partial_\phi \mathbf{Q} = 0$, being \mathbf{Q} a generic spacetime tensor (we can refer to this assumption as the condition of ideal hydrodynamics of equilibrium). The timelike flow vector field u^a denotes now the fluid four-velocity. We investigate in this work in particular the case of a fluid circular configuration on the fixed plane $\sigma = 1$, defined by the constraint $u^r = 0$, as for the circular test particle motion no motion is assumed in the θ angular direction, which means $u^\theta = 0$. We assume moreover a barotropic equation of state $p = p(\varrho)$. While the continuity equation is identically satisfied as consequence of the conditions. The Euler equation for the pressure p can be written

in the non-magnetized case ($B = 0$) as

$$\frac{\partial_\mu p}{\varrho + p} = -\frac{\partial}{\partial \mu} W + \frac{\Omega \partial_\mu \ell}{1 - \Omega \ell}, \quad (5)$$

$$W \equiv \ln V_{eff}(\ell), \quad \ell \equiv \frac{L}{E}, \quad V_{eff}(\ell) = u_t$$

where $V_{eff}(\ell)$ is the *effective potential* Ω is the relativistic angular velocity. Assuming the fluid is characterized by the specific angular momentum ℓ constant (see also Lei et al. (2009)), we consider the equation for W : $\ln(V_{eff}) = c = \text{constant}$ or $V_{eff} = K = \text{constant}$. The procedure described in the present article borrows from the Boyer theory on the equipressure surfaces applied to a thick torus (Boyer 1956; Abramowicz&Fragile 2013). The Boyer surfaces of the **RAD** tori are given by the surfaces of constant pressure or³ $\Sigma_i = \text{constant}$ for $i \in (p, \varrho, \ell, \Omega)$, where it is indeed $\Omega = \Omega(\ell)$ and $\Sigma_i = \Sigma_j$ for $i, j \in (p, \varrho, \ell, \Omega)$.

The function $V_{eff}(\ell)$ in equation 5 is invariant under the mutual transformation of the parameters $(a, \ell) \rightarrow (-a, -\ell)$, as for the case of test particle circular orbits we can limit our analysis to positive values of $a > 0$, for corotating ($\ell > 0$) and counterrotating ($\ell < 0$) fluids. More generally we adopt the notation (\pm) for counterrotating or corotating matter respectively. In the ringed accretion disks system, where a couple (C_a, C_b) of tori are orbiting in the equatorial plane of a central Kerr **BH** with specific angular momentum (ℓ_a, ℓ_b), we need to introduce the concept of *ℓ corotating* tori, defined by the condition $\ell_a \ell_b > 0$, and *ℓ counterrotating* tori by the relations $\ell_a \ell_b < 0$, the two ℓ corotating tori can be both corotating $\ell a > 0$ or counterrotating $\ell a < 0$ with respect to the central attractor.

In the magnetized case, following (Pugliese&Montani 2013; Abramowicz&Fragile 2013; Pugliese&Kroon 2012), we consider an infinitely conductive plasma where $F_{ab}u^a = 0$, and F_{ab} is the Faraday tensor, $u^a B_a = 0$, where B^a is the magnetic field and $\partial_\phi B^a = 0$ and $B^r = B^\theta = 0$. As noted in Komissarov (2006) the presence of a magnetic field with a relevant toroidal component can be related to the disk differential rotation, viewed as a generating mechanism of the magnetic field, for further discussion we refer to (Komissarov 2006; Montero et al. 2007; Horak&Bursa 2010; Parker 1955, 1970; Yoshizawa et al. 2003; Reyes-Ruiz&Stepinski 1999; Safarzadeh et al. 2017), while we refer to (Pugliese&Montani 2013; Adamek&Stuchlik 2013; Hamersky&Karas 2013; Karas et al. 2014; Abramowicz&Fragile 2013) where this solution is dealt in detail in the context of accretion disks. The Euler equation for this system has been exactly integrated for the background spacetime of Schwarzschild and Kerr **BHs** in (Komissarov 2006; Montero et al. 2007; Horak&Bursa 2010) with a magnetic

² We adopt the geometrical units $c = 1 = G$ and the $(-, +, +, +)$ signature, Latin indices run in $\{0, 1, 2, 3\}$. The four-velocity satisfy $u^a u_a = -1$. The radius r has unit of mass $[M]$, and the angular momentum units of $[M]^2$, the velocities $[u^t] = [u^r] = 1$ and $[u^\phi] = [u^\theta] = [M]^{-1}$ with $[u^\phi/u^t] = [M]^{-1}$ and $[u_\phi/u_t] = [M]$. For the seek of convenience, we always consider the dimensionless energy and effective potential $[V_{eff}] = 1$ and an angular momentum per unit of mass $[L]/[M] = [M]$.

³ More generally $\Sigma_{\mathbf{Q}}$ is the surface $\mathbf{Q} = \text{constant}$ for any quantity or set of quantities \mathbf{Q} . In this models the entropy is constant along the flow. According to the von Zeipel condition, the surfaces of constant angular velocity Ω and of constant specific angular momentum ℓ coincide (Abramowicz 1971; Chakrabarti. 1990; Chakrabarti 1991; Zanotti&Pugliese 2015) and the rotation law $\ell = \ell(\Omega)$ is independent of the equation of state (Lei et al. 2009).

field is

$$B^\phi = \sqrt{\frac{2p_B}{g_{\phi\phi} + 2\ell g_{t\phi} + \ell^2 g_{tt}}} \quad \text{or alternatively} \quad (6)$$

$$B^\phi = \sqrt{2M\omega^q} (g_{t\phi}g_{t\phi} - g_{tt}g_{\phi\phi})^{(q-2)/2} V_{eff}(\ell)$$

where $p_B = M(g_{t\phi}g_{t\phi} - g_{tt}g_{\phi\phi})^{q-1}\omega^q$ is the magnetic pressure, ω is the fluid enthalpy, q and M are constant; we assume moreover a barotropic equation of state. Equation 5 has been used in second term of equation 6. According to our set-up we introduce a deformed (magnetized) *Paczynski potential function* and the Euler equation 5 becomes:

$$\partial_\mu \tilde{W} = \partial_\mu [\ln V_{eff} + \mathcal{G}] \quad \text{where} \quad (7)$$

$$(a \neq 0) : \mathcal{G}(r, \theta) = S \left(\mathcal{A} V_{eff}^2 \right)^{q-1} = S (g_{t\phi}g_{t\phi} - g_{tt}g_{\phi\phi})^{q-1};$$

$$\text{and } \mathcal{A} \equiv \ell^2 g_{tt} + 2\ell g_{t\phi} + g_{\phi\phi}, \quad S \equiv \frac{qM\omega^{q-1}}{q-1}$$

parameter S is sketched in Figure 1. We therefore consider the equation for the $\tilde{W} \equiv \mathcal{G}(r, \theta) + \ln(V_{eff}) = K$. The toroidal surfaces are obtained from the equipotential surfaces (Boyer 1956; Pugliese&Montani 2013), where there is

$$\tilde{V}_{eff}^2 \equiv V_{eff}^2 e^{2S(\mathcal{A}V_{eff}^2)^{q-1}} = \quad (8)$$

$$\frac{(g_{t\phi}g_{t\phi} - g_{tt}g_{\phi\phi}) \exp(2S(g_{t\phi}g_{t\phi} - g_{tt}g_{\phi\phi})^{q-1})}{\ell^2 g_{tt} + 2\ell g_{t\phi} + g_{\phi\phi}} = K^2.$$

Potential \tilde{V}_{eff}^2 , for $S = 0$ reduces to the effective potential V_{eff}^2 for the non-magnetized case in equation 5. The equipressure surfaces, $K = \text{constant}$, could be closed, C, determining equilibrium configurations, or open O_\times (related to “proto-jet” configurations (Pugliese&Stuchlik 2016a)). The special case of cusped C_\times equipotential surfaces allows for the accretion onto the central Black Hole, due to the Paczynski-Wiita (P-W) hydro-gravitational instability mechanism occurring at the cusp r_\times , (Paczynski 1980): the outflow of matter through the cusp occurs due to an instability in the balance of the gravitational and inertial forces and the pressure gradients in the fluid, i.e., a mechanism of violation of mechanical equilibrium of the tori—Figure 2. For each torus, the extrema of the effective potential functions fix the center r_\circ , as minimum point r_{\min} of the effective potential and the maximum point for the hydrostatic pressure. The inner edge r_\times of the accreting torus, when accretion occurs, corresponds to the maximum point r_{\max} of the effective potential, also the minimum point for the hydrostatic pressure. The inner and outer edges of an equilibrium torus are also strongly constrained. The inner edge of the Boyer surface is at $r_{in} \in [r_{\max}, r_{\min}]$ on the equatorial plane, while the outer edge is at $r_{out} > r_{\min}$ on the equatorial plane. For a discussion on the definition and location of the inner edge of the accreting torus see (Krolik&Hawley 2002; Bromley et al. 1998; Abramowicz et al. 2010; Agol&Krolik 2000; Paczyński 2000).

In the following, for any quantity \mathbf{Q} and radius r_\bullet we

adopt the notation $\mathbf{Q}_\bullet \equiv \mathbf{Q}(r_\bullet)$, for example there is $\ell_{\text{mso}}^\pm \equiv \ell_+(r_{\text{mso}}^\pm)$. Then 1. for fluid specific angular momentum ℓ in $\mp \ell^\pm \in \mp L_1^\pm \equiv [\mp \ell_{\text{mso}}^\pm, \mp \ell_{\text{mbo}}^\pm]$ topologies (C_1, C_\times) are possible, the C_1 indicated a non-accreting topology C with specific angular momentum $\ell \in L_1$ where $r_\times^\pm \in]r_{\text{mbo}}^\pm, r_{\text{mso}}^\pm]$ 2. for $\mp \ell^\pm \in \mp L_2^\pm \equiv \mp \ell^\pm \in [\mp \ell_{\text{mbo}}^\pm, \mp \ell_\gamma^\pm]$ topologies (C_2, O_\times) are possible, with unstable point $r_j^\pm \in]r_\gamma^\pm, r_{\text{mbo}}^\pm]$. 3. for $\mp \ell^\pm \in \mp L_3^\pm \equiv \mp \ell^\pm \equiv \ell \geq \mp \ell_\gamma^\pm$ only equilibrium torus C_3 is possible.

Similarly to the non magnetized case (where the effective potential is $V_{eff}(r; \ell, a)$), the function $\tilde{V}_{eff}(r; \ell, a, S, q)$ defined in equation 8 may be regarded as an effective potential function encoding the centrifugal and curvature binding effects of the spacetime together with the magnetic pressure force (q), essentially regulated by the S values. Therefore it is important to discuss the range of variation for the (q, S) couple. Section 3.1 addresses further considerations on the parameter choice. We note that a negative solution for S may appear for $q < 1$; we shall briefly consider also the case of tori in this more general situation in section 3.1.

Here we note that, in the limiting case $q = 0$, the magnetic field B , does not depend on the fluid enthalpy, furthermore equation 8 for $q = 0$ is $V_{eff} = K$, this means that the magnetic field $B^\phi|_{q=0}$ does not effect the Boyer surfaces.

It is therefore worth to consider some limits, with the coefficient $\tilde{V}_{eff}^2[n]$ of S^n in the expansion of \tilde{V}_{eff}^2 around $S = 0$:

$$\text{for } S \approx 0 \quad \tilde{V}_{eff}^2[n] = \frac{2^n}{n!} V_{eff}^2 \left(\mathcal{A} V_{eff}^2 \right)^{n(q-1)} \quad n \geq 0,$$

$$\text{thus } \tilde{V}_{eff}^2 = V_{eff}^2 + \frac{2S(\mathcal{A}V_{eff}^2)^q}{\mathcal{A}} + O(S^2) \quad (9)$$

where $O(\mathbf{Q}^K)$ is for terms of the order greater or equal then \mathbf{Q}^K for any quantity \mathbf{Q} . As $S = S(q)$ we consider therefore the coefficient S_n of $(q-1)^n$ in the expansion of S around $q = 1$:

$$S_n = \frac{M \ln^n(\omega)(n + \ln(\omega) + 1)}{\Gamma(n+2)} \quad \text{for } n \geq 0 \quad \text{and } q \gtrsim 1, \quad (10)$$

where $\Gamma(x)$ is the Euler gamma function—Figures 1. In Section 3 we consider in details the case of two magnetized tori orbiting a Kerr central **BH** focusing first on the limiting case of non-magnetized **RAD** system ($S = 0$) of the order two, made up by two orbiting tori.

3 MAGNETIZED RINGED ACCRETION DISKS

We start by solving the equation for the critical points of the function \tilde{V}_{eff} with respect to the fluid specific angular momentum obtaining, similarly to the non-magnetized case the fluid specific angular momentum $\ell^\pm(r)$ replaced by the solution $\tilde{\ell}^\pm(r) : \partial_r \tilde{V}_{eff} = 0$, for counterrotating and corotating magnetized fluids respectively

$$\tilde{\ell}^\mp \equiv \frac{\Delta \left(a^3 + ar \left[4Q(r-M)S\Delta^Q + 3r-4 \right] \mp \sqrt{r^3 \left[\Delta^2 + 4Q^2(r-1)^2 r S^2 \Delta^{2Q+1} + 2Q(r-1)^2 r S \Delta^{Q+1} \right]} \right)}{a^4 - a^2(r-3)(r-2)r - (r-2)r \left[2Q(r-1)S\Delta^{Q+1} + (r-2)^2 r \right]}$$

$$\text{where there is } \lim_{S \rightarrow 0} \tilde{\ell}^\mp = \lim_{q \rightarrow 1} \tilde{\ell}^\mp = \ell^\pm, \quad (11)$$

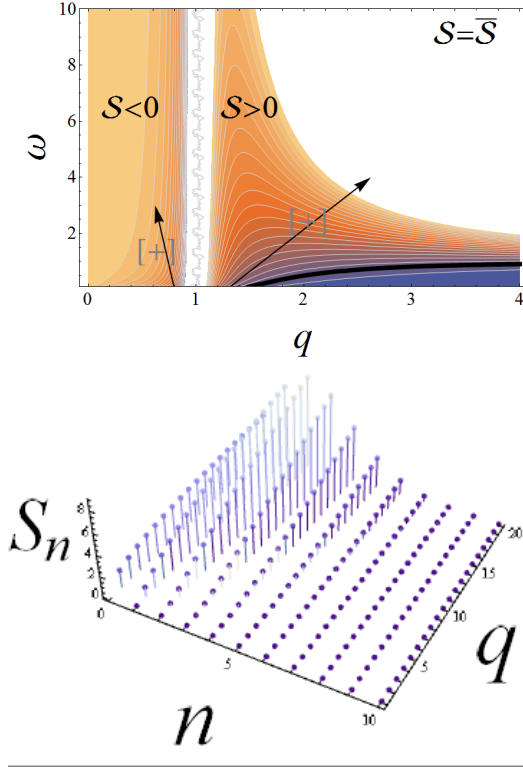


Figure 1. Upper panel: Constant values of $S = \bar{S}$, introduced in equation 7 as function of the fluid enthalpy ω and magnetic parameter q (dimensionless quantities are considered), regions of positive $S > 0$ and negative values $S < 0$ are considered. Black thick line is $S = 0$, arrows mark the increasing values of S parameters. Bottom panel: coefficient S_n of $(q - 1)^n$ in the expansion of S around $q = 1$ —see equation 10, the situation for $q \approx 1$ and $r \rightarrow \infty$, and the limits $S = 1$ and $S = 0$ are shown.

dimensionless quantities $r \rightarrow r/M$ and $a \rightarrow a/M$ have been used—see Figures 3 and Figures 4. We obtained a specific fluid angular momentum expression which explicitly includes the dependence of the field through the S and q parameters. Then, we note also in equation 11 the explicit dependence of ℓ_{\pm} on the parameter $Q = q - 1$ —Figures 3 and 4. Limits 11, furthermore, are consistent with the analysis in equations 9–10 for the asymptotic behavior in the same regions of the parameter space. Therefore we can address the comparison with the non-magnetized case by considering the parameters $S = 0$ or $q = 1$. Nevertheless before to consider the effects of toroidal magnetic field it is appropriate to further comment the situation for the non-magnetized RADs (Pugliese&Stuchlik 2015, 2016a, 2017a).

In the following we consider specific tori couples or *seeds*. As specified in Pugliese&Stuchlik (2016a), the study of these configurations allows both the direct characterization of the system, consisting of only two accretion disks around a central attractor, i.e. a RAD of the order $n = 2$, and it also simplifies the analysis of the more general case of multiple toroidal configurations orbiting a single central attractor. The study of RADs made by more than two orbiting toroidal configurations could be carried out considering composition of *seed* tori couples. Therefore we can concentrate our attention here on two tori with parameters (ℓ_i, ℓ_o) and (K_i, K_o) , for the inner and outer tori respectively with re-

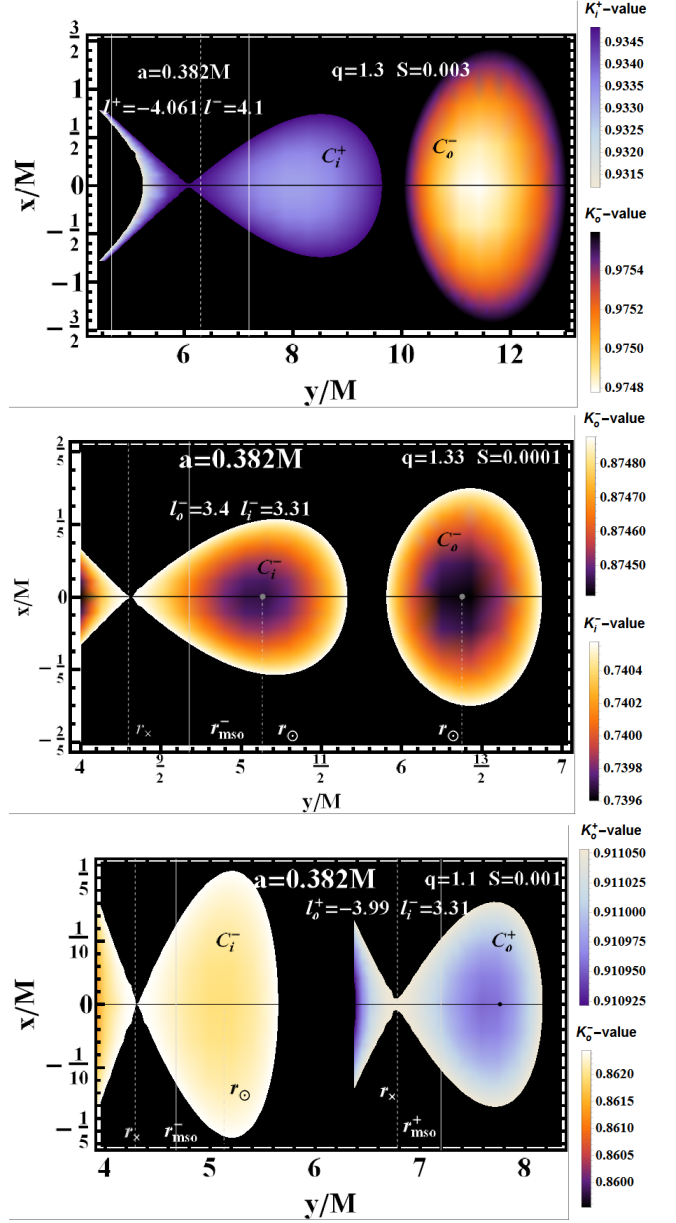


Figure 2. Density plots. *Upper-first panel:* $C_i^+ < C_o^-$ RAD; *Upper-second panel:* $C_o^- < C_o^+$ RAD. *Bottom-panel:* RAD $C_o^- < C_i^+$. (x, y) are Cartesian coordinates. Magnetic parameters (q, S) , BH spin a/M and fluids specific angular momentum are signed (ℓ).

spect to the central BH say, introducing notation \leq , there is $C_i < C_o$ for the relative location of the configurations. The analysis of multiple toroidal disks can be then further simplified by considering appropriate boundary conditions on a properly defined “RAD effective potential” which, for a seed, may be defined as follows for a RADs of the order $n = 2$:

$$\begin{aligned} \tilde{V}_{eff}^{C^2} \Big|_K &\equiv \tilde{V}_{eff}^i \Theta(-K_i) \cup \tilde{V}_{eff}^o \Theta(-K_o), \text{ alternately} \quad (12) \\ \tilde{V}_{eff}^{C^2} &\equiv \tilde{V}_{eff}^i(\ell_i) \Theta(r_o^o - r) \Theta(r - r_+) \tilde{V}_{eff}^o(\ell_o) \Theta(r - r_o^i), \end{aligned}$$

where Θ is the Heaviside (step) function such that for example $\Theta(-K_i) = 1$ for $\tilde{V}_{eff}^i < K_i$ and $\Theta(-K_i) = 0$ for $\tilde{V}_{eff}^i > K_i$.

Note that we adopt the notation $\tilde{\ell}$, for the specific angular momentum in the magnetized case mainly when it is regarded as function of $(r; a, \mathcal{S}, q)$ —equation 11; On the other hand, as when the specific fluid angular momentum is considered as a parameter, for easy of reference, we use simplified notation ℓ , when not otherwise specified—equation 13.

Preliminary notes on the RADs and the non-magnetized case

In the *non-magnetized case*, accreting **RADs** couples may turn in the following four cases *only*: (a) $C_{\times}^{\pm} < C^{\pm}$, (b) $C_{\times}^{+} < C^{\pm}$, (c) $C_{\times}^{-} < C^{\pm}$ and (d) $C_{\times}^{-} < C_{\times}^{+}$. In the case (a), describing ℓ corotating tori or any couple around a static ($a = 0$) attractor, only the inner torus of the couple is accreting onto the central Black Hole. The **RADs** with an ℓ counterrotating couples, distinguish three major classes of **BH** attractors defined by spin ranges with boundaries in geometries characterized by spin $a_1 \equiv 0.4740M$, $a_2 \equiv 0.461854M$ and $a_3 \equiv 0.73688M$ ⁴. Couples $C_{\times}^{+} < C^{\pm}$, (a), and $C_{\times}^{-} < C^{+}$, (c), may form in *all* spacetimes where $a \in [0, M]$ (Pugliese&Stuchlik 2017a). On the other hand, a $C_{\times}^{-} < C_{\times}^{+}$ couple which features a double accretion⁵, (d)-case, can be observed in all Kerr geometries $a \neq 0$, but the slower is the **BH** ($a \lesssim a_1$) the lower must be the specific angular momentum ℓ_{-} of the inner corotating torus and the smaller is the tori spacings. Finally, couples $(\)^{+} < C^{-}$, where $(\)$ stays for an accreting (C_{\times}) or non-accreting (C) torus, (b), can be observable in any spacetime $a \in [0, M]$, although *only* around Kerr attractor with $a \in [0, a_2]$ the corotating, non-accreting, torus C^{-} approaches the instability ($r_{\times} \gtrsim r_{\text{mso}}^{-}$) in the **RAD** seed. Moreover, the faster is the Kerr attractor ($a \gtrsim a_3$), the farther away ($r_{\odot} > r_{\gamma}^{-}$) should be the outer torus to prevent collision (Pugliese&Stuchlik 2017a, 2016a, 2017c). A torus screening effect in this case can occur only with corotating inner screening non-accreting disks. In fact, an accreting *corotating* torus must be the inner one of the couple while the outer counterrotating torus can be non-accreting or in accretion. If there is a C_{\times}^{-} torus, or if the attractor is static, then no inner (corotating or counterrotating) torus can exist, and then C_{\times}^{-} is part of $C_{\times}^{-} < C^{-}$ couple or of a $C_{\times}^{-} < (\)^{+}$ one. A corotating torus can be the outer of a couple of tori with an inner counterrotating accreting torus. Then the outer torus may be corotating (non accreting), or counterrotating in accretion or non-accreting. Both

the inner corotating and the outer counterrotating torus of the couple can accrete onto the attractor. A counterrotating torus can therefore reach the instability being the inner one of any couple, or the outer torus of an ℓ counterrotating couple. Then it is worth noting that if the *accreting* torus is *counterrotating* with respect to the Kerr attractor, i.e. a C_{\times}^{+} , then there is *no* inner counterrotating torus, but a couple may be formed as a $C_{\times}^{+} < C^{\pm}$ or as a $(\)^{-} < C_{\times}^{+}$ one. We propose here the analysis of the four cases for the magnetized fluids by directly integrating the Euler equations, as in Figures 2, and using proper model constraints on the effective potential 12.

The magnetized case

It is convenient to take a closer look at the relation between \mathcal{S} and q . The different dependence of $\tilde{\ell}^{+}$ and $\tilde{\ell}^{-}$, on the parameter couple (\mathcal{S}, q) , is enlighten in Figures 3 and 4.

An important part of our comparative analysis of magnetized and non-magnetized fluids is grounded on the task to verify the presence of any **RAD** systems constraints induced by the magnetic field influence, whose presence here is controlled by \mathcal{S} and q parameters, and viceversa to constraint the couple (\mathcal{S}, q) according to the **RAD** characterization. It was therefore necessary to introduce an adapted function $\mathcal{S}_{crit}(r; \ell, q)$, whose level surfaces, $\mathcal{S}_{crit}(r; \ell, q) = \text{constant}$, provide the values of the parameter \mathcal{S} , for one or two tori. From the equation for the critical points of the hydrostatic pressure, we find $\mathcal{S}_{crit}(r; \ell, q)$ as follows:

$$\mathcal{S}_{crit} \equiv -\frac{\Delta^{-Q}}{Q} \frac{a^2(a - \ell)^2 + 2r^2(a - \ell)(a - 2\ell) - 4r(a - \ell)^2 - \ell^2 r^3 + r^4}{2r(r - 1)[r(a^2 - \ell^2) + 2(a - \ell)^2 + r^3]} \quad (13)$$

(with $r \rightarrow r/M$ and $a \rightarrow a/M$)—see Figure 5. Firstly we note, as in equation 11, the explicit dependence on $Q = q - 1$, and on the quantities $\ell \pm a$ —see also discussion in Pugliese&Montani (2015). We note that a negative solution for \mathcal{S}_{crit} may appear also for $q > 1$ (see Figure 5, however we shall briefly consider also tori with $q < 1$ in section 3.1. More precisely this function of the radius r , the parameter q and the momentum parameter ℓ , represents the values of \mathcal{S} as a function of r , for which critical points of the function \tilde{V}_{eff} exist. In other words it provides indications on the existence of the solutions of the Euler equation, according to our constraints, fixing the radii r_{\odot} and, eventually, for unstable phase, the location of r_{\times} . The existence of a maximum pressure point r_{\odot} is sufficient to establish whether a toroidal solution is possible, while r_{\times} envisages the possible deviation of the equilibrium condition from the non-magnetized case, here the surface $\mathcal{S}_{crit} = 0$. Thus, by analyzing the surfaces $\mathcal{S}_{crit} = \text{constant}$ we are able to assess in quantitative manner the magnetic field influence in the **RADs** formation and instability.

We summarize our findings as follows: generally, **RADs** solutions are possible when the magnetic parameters \mathcal{S} and q are balanced in such a way that their combination remains small enough, i.e. the greater is the $q > 1$ and the smaller has to be \mathcal{S} and viceversa. This fact can be therefore seen an indication of the possible effects of the magnetic field in the direction of suppressing the formation of equilibrium magnetized toroidal configurations. It is then interesting to note the emergence of a relation between the

⁴ The origin of these special spins can be retraced in the geometric properties of the Kerr spacetime and the fluid dynamics, quite independently by the rotational law (specific angular momentum definition)—for more discussion see (Pugliese&Stuchlik 2017a,c; Lei et al. 2009).

⁵ We stress that this special seed is particularly interesting, noting that any **RADs** is to be considered as a geometrically thin accretion disk (Pugliese&Stuchlik 2015). Then only for this special couple a “screening” effect may occur with corotating non-accretion disk between the two accreting tori of the **RAD** (Marchesi et al. 2016; Gilli et al. 2007; Marchesi et al. 2017; Masini et al. 2016; DeGraf et al. 2017; Storch-Bergmann et al. 2017). This mechanism envisages therefore a special “inter-disk” activity with greater potentiality also in view of a possible jet-accretion correlation—see also Pugliese&Stuchlik (2017a,c, 2018) and (Kozłowski et al. 1978; Abramowicz et al. 1978; Sądowski et al. 2016; Lasota et al. 2016; Lyutikov 2009; Madau 1988; Sikora 1981).

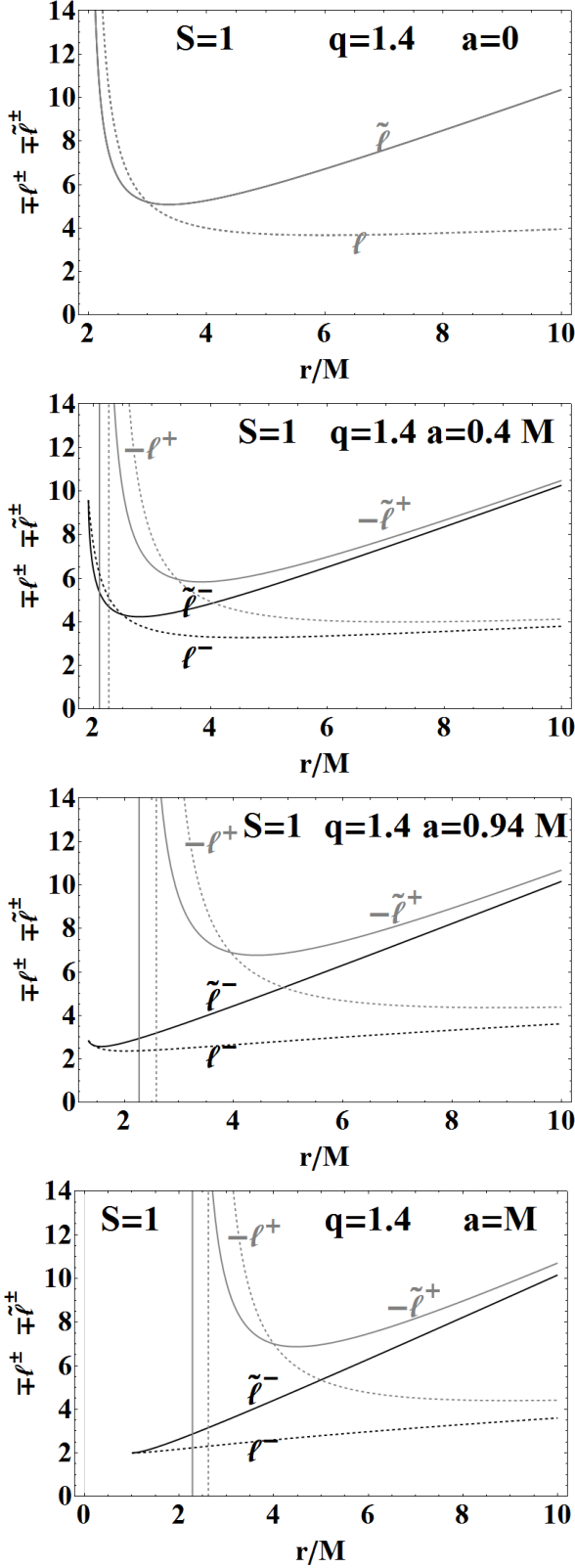


Figure 3. Fluid critical angular momenta $\tilde{\ell}_{\pm}$, in equation 11 for magnetized fluid. Limits ℓ_{\pm} for non-magnetized fluids are also shown, for fixed Kerr BH spin $a \in [0, M]$, magnetic parameters S and q , as function of r/M . The limit of the static Schwarzschild solution for $a = 0$ (where $\ell_{\pm} = \ell$ and $\tilde{\ell}_{\pm} = \tilde{\ell}$) is also shown.

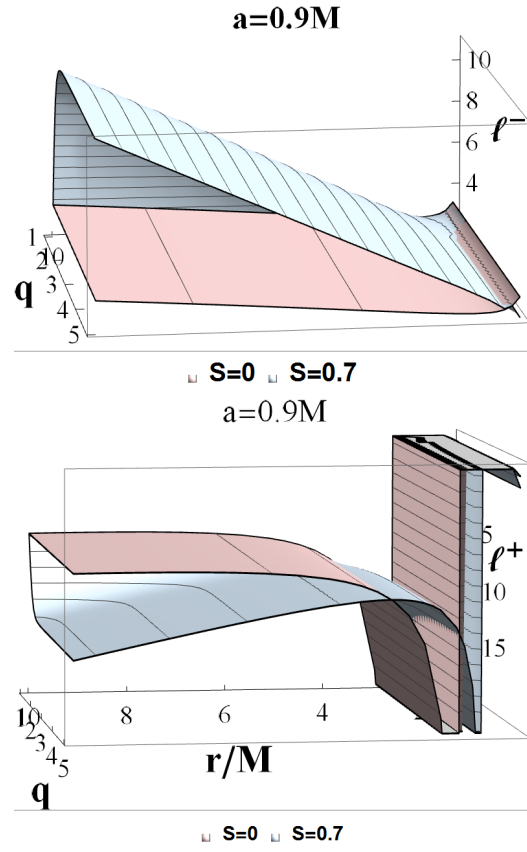


Figure 4. Fluid specific angular momenta $\tilde{\ell}_{\pm}$ (upper panel) and $\tilde{\ell}_{+}$ (below panel) for corotating and counterrotating fluids as function of r/M and magnetic parameter q . Different values of parameters S are considered.

field parameter q and the magnitude S . However both this constraint and the range of variations for q and S actually depend on the BH spin-to-mass ratio and on the relative rotation of the orbiting fluids. Remarkably this analysis has proved also the different behavior of $\ell_{\text{counterrotating}}$ and $\ell_{\text{corotating}}$ tori in presence of toroidal magnetic field, which is also particularly evident in range $q < 1$ considered here in the sideline of this investigation in section 3.1– Figures 7. Concerning the analysis for $q > 1$, as clear from Figures 6, there is $S_{\text{crit}} \in [0, S_{\text{max}}]$, that is S is bounded below by the non-magnetized case and above by a maximum value S_{max} , which however is not always present—see Figures 6—second from above. The situation depends mostly on the relative rotation of the fluids and also from the BH spin. It can be shown that the maximum value S_{max} depends linearly on q . A systematic study of the solutions in all the parameters space, which would imply the combined selection of different ranges of parameters is left here for future investigation: however we can note that the presence of maximum for S_{crit} is related to the presence of instabilities, consequently this study provides also constraints on the emergence of P-W instability and on the relevance of the toroidal magnetic fields contribution in enhancing accretion. Figures 6 show some exemplary cases. Integrations of Euler equation for a couple of magnetized tori in fixed spacetimes are in Figures 2. As mentioned above, these analysis confirm the requirement of small values of qS , it follows that the magnetic field is

strongly constrained by the torus formation: the presence of a strong field in the early age of accretion disk evolution would act in direction to suppress the torus formation—Figures 6. Comparing then with the $S = 0$ case, we see that the instability points shift away from the central attractor which implies that the magnetic field has essentially in general a destabilizing effect on the configurations, fostering the instability emergence. Then the accreting magnetized tori are generally smaller (equatorial plane elongation) than the non magnetized ones. Asymptotically, for large values of r , the parameter S decreases to zero values for $q > 1$. In particular, this means that a magnetized torus may form close to the central attractor. Focusing on the ℓ corotating couples, we note that S increases with the magnitude of ℓ moving the torus and the maximum of S inwardly. This trend is due to the coupling between the centrifugal and the magnetic field component of the force balance in Euler equation, encoded in the effective potential function \tilde{V}_{eff} in equation 8. The magnetic pressure in equation 6 is independent from the fluid specific angular momentum ℓ , viceversa the magnetic field B_ϕ explicitly depends on ℓ through \lesssim in equation 7. The greater is the fluid rotation and the greater is the magnetic field, increasing the maximum $S_{crit} = S_{max}$ values and the radius r_i : $S_{crit}(r_i) = S_{max}$ for the case of $S = 0$. This behavior is substantially independent from the sign of rotation with respect to the central attractor— for the corotating and counterrotating couples of ℓ corotating tori— see Figures 6. Fluid rotation would act therefore so to offset the effects of the magnetic field. Considering then the ℓ corotating fluids, **RADs** may form at equal q and S —constant lines in S_{crit} in Figures 6—Figures 5. This would be an important indication in support of the **RADs** origin, with constrained angular momentum, from one common embedding material as envisaged in (Pugliese&Stuchlik 2015, 2016a, 2017a). The magnetic field would act so as to foster the formation of a single accretion disk, following the emergence of **RAD** instability originating from each torus unstable phases or from tori collision. It is clear then that in the ℓ corotating couples, the maximum common value of the parameters S for the tori to be considered is $S = S_i$ relative to the inner torus.

The ℓ counterrotating magnetized fluids constitute a particular interesting case where, for $S = 0$, couples $C_x^+ < C_x^-$ and $C_x^- < C_x^+$, might occur. As clear from Figures 6 the following two cases may occur: *i.* there is partial or total overlapping of the curves S_- (for the inner torus) and S_+ , and in this case the situation for a **RAD** is analogue to the ℓ corotating case discussed above. *ii.* The second case consists of S_{crit} curve profiles which are totally disjoint, as in Figures 6—third line. In general in the ℓ counterrotating case we can assess the different coupling between the centrifugal component and the magnetic field contribution in the counterrotating and corotating cases respectively (for $a \neq 0$) (and this is especially clear for the case $q < 1$, which is also addressed in Sec 3.1). The presence of a toroidal magnetic field would distinguish between corotating and counterrotating fluids, favoring the formation of the first (Volonteri et al. 2003). In the ℓ counterrotating couples, if there is no maximum S_{max} the curves are overlapped as they are always in the ℓ corotating case, implying that tori at equal S and q are always possible, and this may support the possibility of common origin for the tori. In the case of disjointed curves, the common S_{crit} parameter would be determined by the

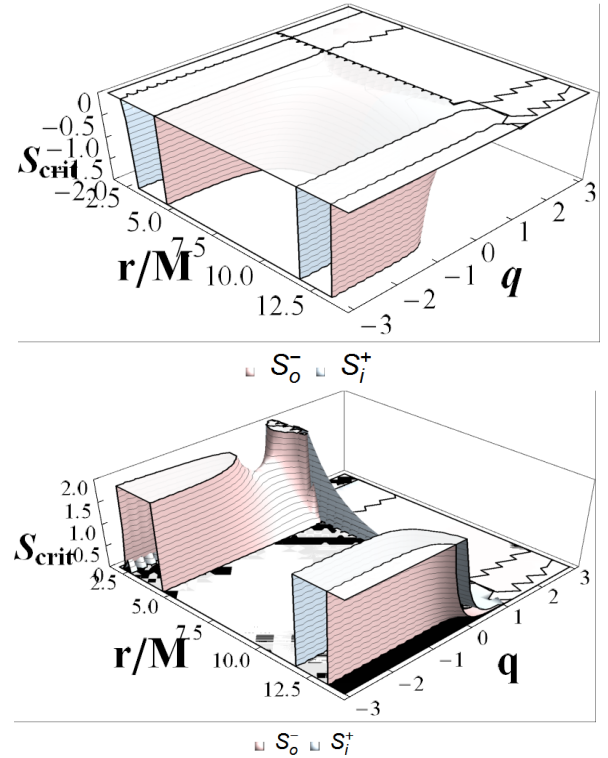


Figure 5. Function $S_{crit}(r; a, \ell, q)$ introduced in equation 13 as function of radius r/M and magnetic parameter q , for fluid specific angular momentum ℓ_\pm (equation 11) for S_\pm respectively according to fluid rotation. The **BH** spin is $a =$, fluid specific angular momentum $\ell^- = 4.01$ and $\ell^+ = -4.4$, $a = 0.382M$, for negative (positive) values of $S_{crit}(r; a, \ell, q)$ upper panel (below panel). See also Figures 6).

external counterrotating torus. This suggests a different origin for the tori of an ℓ counterrotating couple in the case $C_- < C_+$ only (Pugliese&Stuchlik 2017a).

3.1 Some considerations on the parameter choice

In this section we further discuss the parameter choice focusing on the range of variation for the q -parameter. We have seen from equations 7-8 and equations 11-13, that the **RADs** strongly depend on the parameter $Q = q - 1$. We assumed $Q > 0$, with $Q = 0$ matching the limiting case for null magnetic component. Considering again Euler equation 5, with the effective potential \tilde{V}_{eff} in equation 8 including the magnetic contribution, we can note that Q parameter in fact defines positive or negative contribution of the magnetic pressure in the pressure-force balance, together with the barotropic pressure contribution and the centrifugal and gravitational parts, included in the (non-deformed) effective potential V_{eff} . In here we briefly discuss results of the analysis performed in this extended parameter ranges considering a negative Q —see Figures 7.

We can clearly see the presence of maxima and of possible negative values (for $q < 1$) of the parameter⁶ Q —Figure 7. The first relevant feature in this new set-up consists in the

⁶ This special choice of S (M) and q parameters requires a throughout discussion of the matter and fields characteristic as

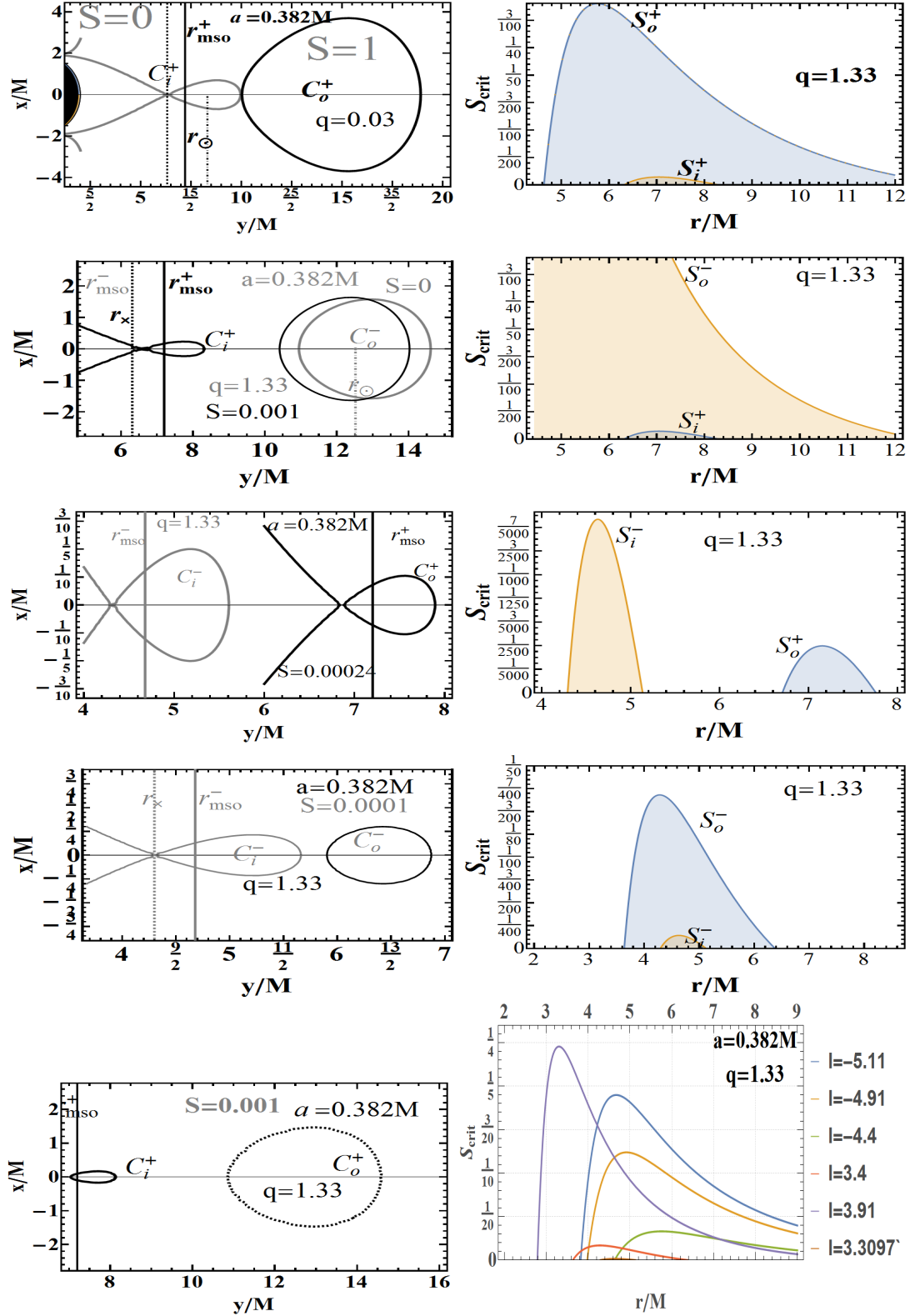


Figure 6. Left: Cross sections, on the equatorial plane, of the outer Boyer surfaces (Roche lobes) for ℓ counterrotating and ℓ corotating tori orbiting a central Kerr BH (left and bottom panel), and associated S_{crit} parameter (right panels) as function of r/M —see also equation 13. (x, y) are Cartesian coordinates. Bottom panel: $S_{crit}(r; a, \ell, q) > 0$ for different values of momentum ℓ_{\pm} .

possible formation of a multi-tori where both **RAD** accretion disks have the same ℓ and K values, which obviously cannot be in the case of different magnetic parameter values. This implies that each torus is not uniquely defined, in general, in this range values for the magnetic parameter, by the only fluids rotation ℓ and density K parameters. Moreover, this suggests also that the same original matter, constituting the primordial embedding of the disks, may probably give rise to two different accretion tori with equal centrifugal (ℓ), density (K) and magnetic (Q) properties, eventually pointing out an interesting mechanism in the disk formation. The second, relevant difference with respect to the other **RADs** considered here, consists in the fact that, for the inner torus, so-called excretion phase is possible. This mechanism of the accretion disks instability is indeed a well known feature of different scenario as in (Stuchlik et al. 2015; Stuchlik 2005; Stuchlik et al. 2009; Stuchlik&Kovar 2008; Kucáková et al. 2011; Slaný & Stuchlik 2005; Adamek&Stuchlik 2013). In excretion disks the balance of forces is such that the flow starts from the center of the disk and exits the outer margin (in this sense we could say there is a role shift between the outer r_{out} and the inner r_{in} edge). Excretion disks form for example at stars merging. However, in all the different circumstances considered in the former studies, a repulsive effect in the force balance appears, generally inherited as a peculiar feature of the background geometry, therefore enucleated in the gravitational part contribution of the effective potential in the forces-balance equation. In our case, in this extended range of the Q parameter, interestingly, the repulsive effect is in fact introduced directly in the balance of the forces, due to the magnetic field contribution. These multiple configurations, seen as a very special subgroup of **RADs**, would emerge for the counterrotating configurations only. This situation leads us to conjecture that a general classification of balance of forces in tori may be done, answering to the question of how should be the effective potential modified to envisage such kind of special multi-tori with equal parameter values and where excretion processes may occur. Then, the existence of these solutions, will let us to conclude that existence of any excreting tori in fact may not be exclusively attributed to the effects of a *geometric repulsive force*, due to a cosmological constant contribution (Stuchlik 2005; Stuchlik et al. 2009; Slaný & Stuchlik 2005; Stuchlik&Kovar 2008), to some kind of quantum distortion effects having such impact on the larger scales (Stuchlik et al. 2015), or the presence of super-spinning sources (Adamek&Stuchlik 2013; Stuchlik&Schee 2013; Stuchlik& Schee 2010; Stuchlik et al. 2011) for example. These orbiting tori may therefore represent more common situations in Astrophysics, then fol-

described by these values, and the implication on the conservation equations, the Komissarov field and, importantly, the **RADs** components boundary conditions, which are here particularly relevant as excretion disks may appear. This analysis is left for future investigation. However, without over-deepening this aspect that eludes the purposes of the present analysis, we can say that a study of the S_{crit} quantity as in Figures 5 reveals a far more rich scenario than the cases depicted in Figures 6 and Figures 7; we can consider the negative S_{crit} values, defined in equation 13, giving rise to accretion disks or, negative Q , which gives rise to toroidal solutions of Figures 7 satisfying the requirement of constant (magnetized) potential.

lowing assumptions on very special and exotic backgrounds. Particularly they may be relevant in the early phases (as transient stages) of the accretion disks formation. This hypothesis encourages for future analysis directed towards the investigations of these cases.

4 NOTES ON THE RAD INSTABILITIES

In this section we add some further comments on the stability of the **RADs** configurations constituted by tori endowed with a toroidal magnetic field. We briefly consider also the possible observational implications associated with the instabilities.

RAD instabilities should be treated in accordance with a global point of view where the macrostructure is considered as a single, unique disk orbiting around a central **SMBH**. In the construction of the **RAD** model, presented in Pugliese&Stuchlik (2015), special attention has been given to the development of the **RAD** as an whole, geometrically thin disk. In fact, the current interpretative framework of the **BH**-accretion disk physics generally foresees the scenario of a **BH**-one disk system. Consequently we should consider the possible situation of a “**RAD** in disguise”, i.e. a **RAD** could be observed as a geometrically thin, axis-symmetric disk, centered on the equatorial plane on a Kerr **SMBH**, with a “knobby” surface and characterized by a differential rotation with peculiar optical properties. (Optical properties of a couple of orbiting tori are expected to be investigated in a future work, on the other hand X-ray emission are expected to shown the ringed structure in a discrete emission profile—see for example Sochora et al. (2011); Karas&Sochora (2010); Schee&Stuchlik (2009, 2013).) It is clear then that the instability of each **RAD** component must reflect in an inter-**RAD** disk activity. More in general, the **RAD** instabilities have been classified into three main processes: (i) a destabilization of the system may arise after the emergence an instability phase of one component of the **RAD**, for example after an accretion phase of one torus onto the central **BH** or the proto-jet emission which is capable to destabilize the entire disk (Pugliese&Stuchlik 2018, 2017b). This case however has been strongly constrained. As discussed in Section 3, in any **RAD** the maximum number of accreting tori is $n_x = 2$, occurring for the couple $C_x^- < C_x^+$, made by an inner corotating and outer counterrotating torus accreting on the **BH**. (ii) A **RAD** can be destabilized after collision of a pair of quiescent tori of the agglomeration. Collision may arise for example after growing of one torus Pugliese&Stuchlik (2017a,c). (iii) In the couple $()^- < C_x^+$, the accretion phase of the outer torus, (i)-instability, and the collision emergence, (ii)-instability, can combine establishing a complex phase of **RAD** destabilization. This situation has been discussed in Pugliese&Stuchlik (2015), where **RAD** perturbative approaches have also been described. In Pugliese&Stuchlik (2016a), the emergence of unstable tori have been detailed, while further discussion on **RADs** as remnants of **AGN** accretion periods are in Pugliese&Stuchlik (2018). The particular case of the emergence of collision for two **RAD** tori was considered in Pugliese&Stuchlik (2017a). Interacting tori and energetic of associated to these processes were investigated in Pugliese&Stuchlik (2017c). In this analysis

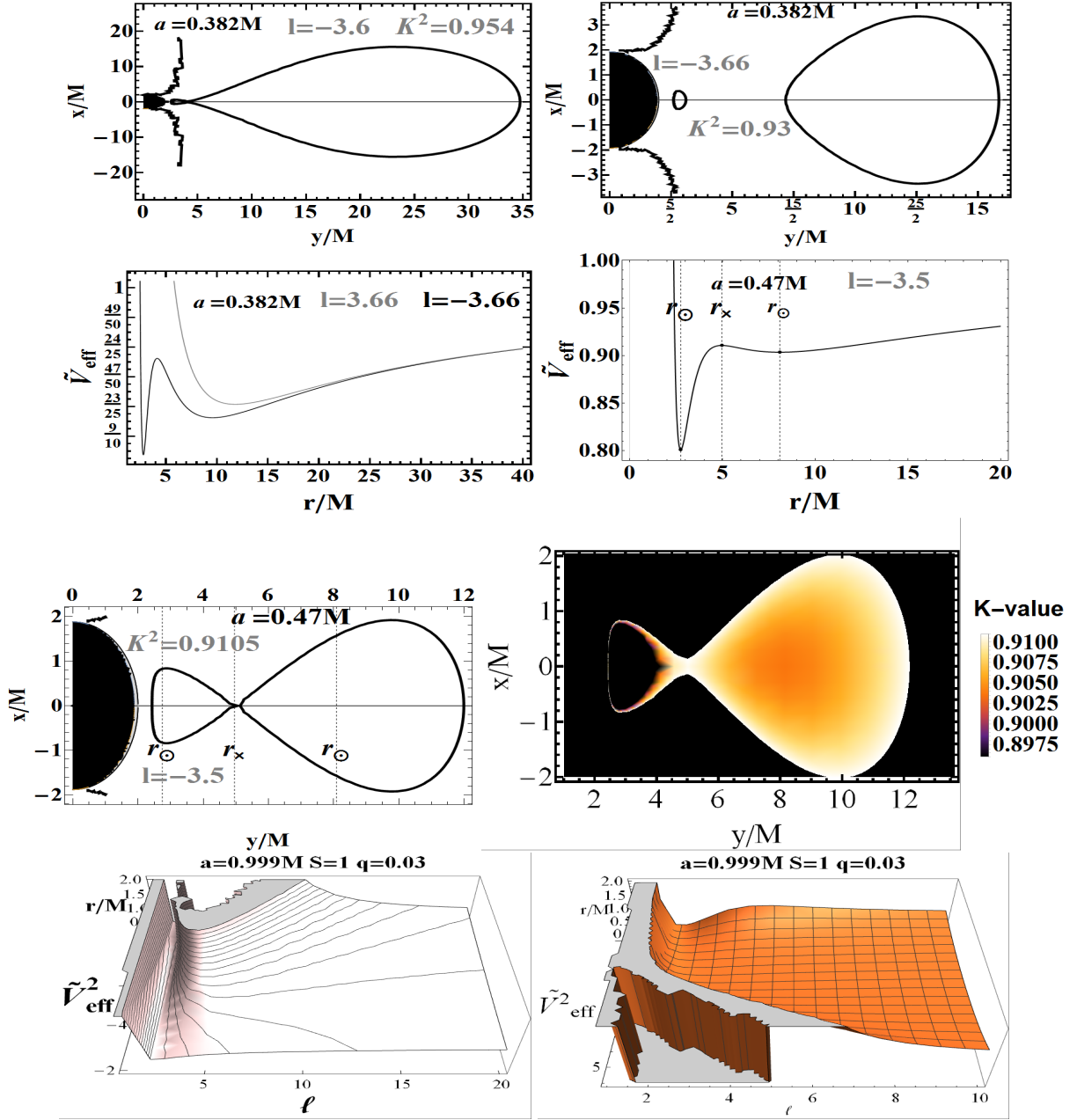


Figure 7. Case $q \in [0, 1[$ ($Q < 0$): Upper and middle panel-lines: the closed Boyer surfaces at K^2 and ℓ fixed and associated effective potential ($S = 1$). Disk center r_\odot and critical points r_x are also signed. Third line panel: density plot. Double accretion configurations appear. Bottom panels: different view of the effective potential as function of fluid specific angular momentum ℓ and radius r/M . Double minima appear for a restricted region of parameter value $\ell < 0$. (x, y) are Cartesian coordinates. Black region is $r < r_+$, r_+ is the Black Hole horizon.

the energy released during the collision of two adjacent tori, $C_x^- < C_x^+$ or $C_x^+ < C_x^\pm$, has been evaluated. The mass accretion rates, the luminosity at the cusps and other fundamental characteristics of the BHs accretion disk physic were also evaluated. From the phenomenological viewpoint, the shift in paradigma from the interpretative framework of the BH-disk interaction to the BH-RAD clearly opens a broad scenario of investigation focusing, on one side, on the special phenomena associated to the RAD instabilities, as the occurrence of double accretion and its after-dynamics, the

inter disks proto-jet emission and the screening tori; on the other side, the RAD model opens the possibility to review the main template of analysis from a SMBH-disk framework to a SMBH-RAD one. More precisely, concerning the phenomenology connected to the (i), (ii) and (iii) instabilities, the analysis in Pugliese&Stuchlik (2017c) suggests that such phenomena can be associated with release of high energy emissions. Then from the point of view of the agglomerate, the collision instability can lead to different evolutive paths for the aggregate tori, depending on the initial con-

ditions of the processes as the torus rotation with respect to the black hole, the range of variation of the mass of the torus and of the magnitude of the specific angular momentum of the fluids. A possibility consists in the formation of in a single torus, in fact canceling the **RAD** structure, explaining mainly in the first evolution phases of the formation of the aggregate. We should also note that, as pointed out in [Pugliese&Stuchlik \(2017a\)](#), an inner torus of the orbiting **RAD** couple may form as axially symmetric corotating toroidal disk after a first phase of formation of the outer aggregate component.

Conversely, another possibility is the occurrence of a “drying-feeding” phase, involving interrupted stages of accretion of one or two tori of a couple. In this case, matter flows between the two tori of the couple, accretion being interspersed with equilibrium phases, eventually giving raise to a series of interrupted stages of accretion onto the central **SMBH**. This particular effect, considered in [Pugliese&Stuchlik \(2017a, 2018\)](#) and detailed in [Pugliese&Stuchlik \(2017c\)](#) can represent a fitting environment for the different phases of super-Eddington accretion advocated as a mechanism to explain the large masses observed in **SMBHs** at high redshift—see for example [Volonteri et al. \(2007\)](#); [Volonteri \(2007, 2010\)](#); [Li \(2012\)](#); [Oka et al. \(2017\)](#); [Kawakatu&Ohsuga \(2011\)](#); [Allen et al. \(2006\)](#). In the case of a $(- < C_x^+ < C^+)$ system the inner, accreting or quiescent, torus can be an obscuring inner torus. Matter, from the outer counterrotating torus, impacts on the corotating inner one, which is screening the accretion from the central **SMBH**. The possible evolutive paths of such system have been constrained in the hydrodynamics case using constraints on the variation ranges of the **RAD** parameters and on Eq. (8)—[Pugliese&Stuchlik \(2017a\)](#). This treatment is semi-analytic, while the full evolution of the collisional regime has to be considered apart.

More generally, each torus oscillation mode will reflect on the **RAD** structure adding up to those of other components of the agglomerate, each torus will contribute with its own specific characteristic. Eventually this can be also related to **QPOs** emission—see [Montero et al. \(2007\)](#). It is therefore necessary to consider the oscillations and instabilities associated with the each component of the aggregate. The introduction of a purely toroidal and even small magnetic field (considering the magnetic pressure *versus* gas pressure as defined by the β -parameter) can have influence on the development of these modes. This is relevant particular for the the torus global non-axis-symmetric modes, because of the generation of the Magneto-Rotational Instability (MRI) due to the magnetic field and fluid differential rotation. Geometrically thick discs are subjected to several oscillation modes: a first modes set is constituted by incompressible and axis-symmetric modes which correspond to global oscillations for radial, vertical and epicyclic frequencies together with surface gravity, acoustic and internal modes which are recovered from the so called relativistic Papaloizou-Pringle (**PP**) equation—see for example [Abramowicz&Fragile \(2013\)](#). On the other hand, the Papaloizou-Pringle Instability (**PPI**), is a global, non-axis-symmetric instability which is able to transport angular momentum outwardly in the disk and therefore able to finally trigger the accretion. The global non-axis-symmetric hydrodynamic (**HD**) **PPI** implies also the formation of long-

lasting, large-scale structures that may be also tracer for such tori in the in the gravitational wave emission—see for example [Kiuchi et al. \(2011\)](#). We also note that the presence of these modes in complex structures such as those provided by the **RAD** can be extremely intriguing, considering the possibility of the emergence from distinct structures belonging to the aggregate, which are characterized by fluids with different physical proprieties.

Accretion in **BH** disks is provided by an instability process which is able to trigger the matter overflow in the torus. In the geometrically **HD** thick disks, the accretion process is strictly interwoven with the development of the **PP** instability: the mass loss in the Roche lobe overflow regulates the accretion rate in the innermost part of torus. This self-regulated process on one side locally stabilizes the accreting torus from the thermal and viscous instabilities and, on the other side, it globally stabilizes the torus from the **PPI**—([Abramowicz 1981](#); [Blaes 1987](#)). (Note also that the amount of overflow may be also modulated by global disks oscillations.) In fact, global instabilities are affected by the boundary conditions assumed for the system. In the case of **PPI** in **RAD** accreting **HD** tori, for which the disk inner and outer edges are well defined and located, the **PPI** is generally suppressed, stabilizing the disks by the accretion flow driven by the pressure forces across the cusp, r_x , according to the mechanism considered in Section 2. In the case of geometrically thick torus endowed with a (purely) toroidal magnetic field, considered here with the analytic Komissarov solution, a series of recent analysis shows that torus is violently prone to develop the non-axisymmetric MRI in 3D which could disturb this configuration on dynamical timescales—see [Del Zanna et al. \(2007\)](#); [Wielgus et al. \(2015\)](#); [Das et al. \(2017\)](#) and [Bugli et al. \(2017\)](#). The **PPI** hydrodynamic instability is entangled with an emerging MRI which triggers eventually predominant larger modes of oscillation (smaller length scales) with respect to typical **PPI** modes, and creating a far richer and complex scenarios for the torus equilibrium properties. Therefore, the presence of a magnetic field contribution in the disk force balance leads to a more complex situation where the **PPI** has to be considered in a broader context. More generally, whether or not the hydrodynamical oscillation modes in MHD geometrically thick disks may survive such global instabilities or the presence of a weak magnetic field would strongly affects these, is still under investigation. The linear development of the **PPI** can be affected by the presence of a magnetic field and by a combined growth of the MRI. These two processes can coexist, enter into competition and combine depending on local parameters of the model (strongness of the magnetic field as evaluated by β parameter). Some studies seem to suggest that under certain conditions on the strength of the magnetic field and other conditions on the torus onset, this situation can also be resolved in the **PPI** suppression by the MRI in the relativistic accretion disks. Using three-dimensional GRMHD simulations it is also studied the interaction between the **PPI** and the MRI considering an analytical magnetized equilibrium solution as initial condition ([Bugli et al. 2017](#)). In the **HD** tori, the **PPI** selects the large-scale $m = 1$ azimuthal mode as the fastest growing and non-linearly dominant mode. In different works it is practically shown that even a weak toroidal magnetic field can lead to MRI development which leads to the suppression of the

large-scale modes. Notice also that the magneto-rotational instability in the disks is important because disks can be locally **HD** stable (according to Rayleigh criterion), but they are unstable for **MHD** local instability which is linear and independent by the field strength and orientation, and growing up on dynamical time scales. The torus (flow) is **MHD** turbulent due to the MRI. The MRI process induces an angular momentum transfer towards the outer region of the torus using the torque of the magnetic field lines. In the magnetized tori, as the **RAD** tori considered here, the accretion is triggered at much earlier times than in the **HD** tori, and modes higher than the azimuthal $m = 1$ mode, typical of **HD-PPI** tori, emerge together with $m = 1$. GRMHD investigations show generally an increase of turbulent kinetic energy in the earlier phases competing with the GRHD ones, consequently accretion is in fact triggered by the Maxwell stresses instead of the **PPI**. Furthermore, in the magnetized case there is a broader range of excited frequencies with respect to the GRHD model. Eventually the fundamental mechanism responsible for the onset of the **PPI** does not appear to be the predominant one or even to arise at all in the MHD torus. In conclusion these works show that the inclusion of a toroidal magnetic field could strongly affect, even with a sub-thermal magnetic field, the **PPI**. Ultimately there are suggestions that the action of MRI suppresses the **PPI** $m = 1$ mode growth. This may have a relevant consequence in the double **RAD** system. MRI stabilizes the disks to **PPI** with **MHD** turbulence. Firstly in general MRI is more effective and faster in transport of angular momentum across the disk, and higher accretion rates were proved to occur in the magnetized models. The evaluation of the accretion rates in the GRHD double **RAD** systems has been carried out in [Pugliese&Stuchlik \(2017c\)](#). The emergence of the MRI suggests an accentuation of the effects of the (i) and (iii) instabilities, whereas we do not expect the principal mechanisms to be changed but rather to accentuate those phenomena connected with energy release and matter impact. Nevertheless these consideration have to be dealt with the constraints provided in Section 3. Finally it should be noted that, according to [Fragile&Sadowski \(2017\)](#), strong toroidal magnetic fields are rapidly suppressed in this tori, in favor of weaker fields (decrease of β parameter). On the other hand, despite these investigations seem to converge towards a quite clear picture of the MRI-**PPI** interaction in geometrically thick disks, although indicative of what the situation could be in general, more analysis is definitely needed to draw a more conclusive picture of this interaction. The relative importance of MRI and **PPI** and the interaction of two processes depends in fact on many factors and conditions. In particular in the **RAD** scenario different factors can be determinant: the (turbulent) resistivity, the emerging of a dynamo effect, the study for counterrotating (retrograde) tori, the disk self-gravity, the gravitational interaction between the disk and the central Kerr **SMBH** and the runaway instability are further aspects which may contribute importantly to the characterization of the ongoing processes.

5 CONCLUSIONS

We studied the effects of a toroidal magnetic field in the formation of multi-magnetized accretion tori in the ringed accretion disks (**RADs**), orbiting around one central super-massive Kerr Black Hole. Results constitute evidence of a strict correlation between **SMBH** dimensionless spin, fluid rotation and magnetic fields in **RADs** formation and evolution towards instability. We showed how the central **BH** dimensionless spin, the presence of a magnetic field and the relative fluid rotation and the rotation with respect the central attractor, play a crucial role in determining the accretion tori features. Specifically, it is proved that toroidal magnetic field and disks rotation are strongly related. This can ultimately have a major influence in the **BH**-accretion disk systems, especially during the early stage of tori formation and the final steps of evolutions towards the accretion onto the spinning **BH**, a phase where predominant instabilities occur for the accreting torus as well as for the **RAD** system. Noticeably, we found that only specific classes of constrained tori, for restrict ranges of magnetic field parameters may form around special **SMBHs** belonging to classes identified by their dimensionless spin. This clearly has huge implications for observational point of view, providing indications on the contexts where to observe such configurations, providing also insight on the different stages of the **BH** life interacting with its environment and the torus features. In section 3 we provided a detailed summary of the findings. Only for **BHs** with spin parameter $a \neq 0$ and in a couple made by an outer counterrotating torus and inner corotating torus, a double accretion occur, with the outer accreting matter impacting on the inner “screening” disk, which is also accreting onto the central **BH**. This mechanism envisages a special “inter-disks” activity with greater observational potentiality and it poses strict constraints of the current studies of X-ray emission screening in **BH** environments, restricting strongly the situations where a screening effect from an orbiting inner tori can be considered ([Marchesi et al. 2016](#); [Gilli et al. 2007](#); [Marchesi et al. 2017](#); [Masini et al. 2016](#); [DeGraf et al. 2017](#); [Storchi-Bergmann et al. 2017](#)). The possibility of tori collision under the effect of the magnetic field is also enlighten for a system of non-accreting couple and for impact of matter inflow from the outer onto the inner disk. A modification of the tori rotation law (specific angular momentum), depending on the magnetic field is discussed. This has the advantage to provide a fairly small, though detailed, template of associated phenomenology, with special regard to situations where collisions and accretion occur. The counterrotating and ℓ counterrotating cases show significantly that the toroidal magnetic field plays an essential role in determining the disk structure and stability, showing that also a purely azimuthal field is capable to discriminate the **RAD** features. From a methodological point of view, the rewriting of Euler equations in the form of an equation with an (general relativistic) effective potential allows us to precisely estimate the balance of each component of the forces regulating the disk and the **RADs** agglomerate. In the choice of a particular set-up, especially for a magnetized model, there is inevitably a level of arbitrariness in the specification of the model ending up to narrow the range of situations where this can fit to very specific contexts. The single magnetized torus of **RAD** is however widely used to

fix up the initial configurations for numerical integration of a broad variety of **GRMHD** models. Parameterizing the magnetic field through the two parameters (q, \mathcal{S}), we narrowed the range of parameter variation, relating the \mathcal{S} parameter values to the system critical points.

In conclusion, the results of our analysis show that the magnetic field has an important role in determining the **RADs** formation and instability. In this respect, as we already stressed in Section 3, we should in fact revisit the current analysis of screened X-ray emission, by considering constraints provided here on the formation of an inner screening torus.

DP acknowledges support from a Junior GACR Grant of the Czech Science Foundation No:16-03564Y. This work has been developed in the framework of the CGW Collaboration (www.cgwcollaboration.it).

REFERENCES

- Abramowicz M. A., 1971, *Acta. Astron.*, 21, 81
 Abramowicz, M. A. 1981, *Nature*, 294, 235–236
 Abramowicz M. A. & Fragile P. C., 2013, *Living Rev. Rel.*, 16, 1
 Abramowicz M. A., Jaroszynski M., Kato S. et al., 2010, *A&A*, 521, A15
 Abramowicz M.A., Jaroszynski M. & Sikora M., 1978, *A&A*, 63, 221
 Agol E. & Krolik J., 2000, *ApJ*, 528, 161
 Adamek K. & Stuchlik Z., 2013, *Class. Quantum Grav.* 30, 205007
 Allen, S. W., Dunn, R.J.H., Fabian, A.C., et al 2006, *MNRAS*, 1, 372, 21
 Aly H., Dehnen W., Nixon C. & King A., 2015, *MNRAS*, 449, 1 65
 Alig C., Schartmann M., Burkert A., & Dolagapj K., 2013, *ApJ*, 771, 119
 Balbus S. A. 2011, *Nat.*, 470, 475
 Balbus S. A. & Hawley J. F., 1998, *Rev. Mod. Phys.*, 70, 1
 Blaes O. M., 1987, *MNRAS*, 227, 975–992
 Blanchard P. K. *et al.*, 2017, *arXiv:1703.07816*
 Boyer R. H., 1956, *Proc. Cambridge Phil. Soc.*, 61, 527
 Bromley B. C., Miller W. A. & Pariev V. I., 1998, *Nature*, 391, 54, 756
 Bugli M., Guilet J., Muller E., Del Zanna L., Bucciantini N., Montero P. J., 2017, *ArXiv e-prints*, 1707.01860
 Carmona-Loaiza J. M., Colpi M., Dotti M. & Valdarnini R., 2015, *MNRAS*, 453, 2, 1608
 Chakrabarti, S. K., 1990, *MNRAS*, 245, 747
 Chakrabarti S. K., 1991, *MNRAS*, 250, 7
 Colgate S. A., Li H. & Pariev V., 2001, *Phys. Plasmas*, 8, 2425
 Cremaschini C. & Stuchlik Z., 2013, *Phys. Rev. E*, 87, 043113
 Das U., Begelman M. C. & Lesur G., 2017, *MNRAS*, 473, 2791
 DeGraf F., Dekel A., Gabor J. & Bournaud F., 2017, *MNRAS*, 466, 2, 1462
 Del Zanna L., Zanotti O., Bucciantini N., Londrillo P., 2007, *A&A*, 473, 11
 Dyda S., Lovelace R. V. E., Ustyugova G. V., Romanova M. M. & Koldoba A. V., 2015, *MNRAS*, 446, 613
 Fragile P. C. & Sadowski A., 2017, *MNRAS*, 467, 1838
 Gilli R., Comastri A. & Hasinger G., 2007, *A&A*, 463, 79
 Gimeno-Soler S. & Font J. A., 2017, *A&A*, 607, A68
 Grasso D. & Rubinstein H. R., 2001, *Phys. Rept.*, 348, 163
 Horak J. & Bursa M., “Polarization from the oscillating magnetized accretion torus,” in R. Bellazzini, E. Costa, G. Matt & G. Tagliaferri *X-ray Polarimetry*, Cambridge University Press (2010) *arXiv:0906.242*
 Hamersky J. & Karas V., 2013, *A&A*, 555, A32
 Karas V. & Sochora V., 2010, *ApJ*, 725, 2, 1507–1515
 Karas V., Kopáček O., Kunneriath D. & Hamerský J., 2014, *Acta Polytech.*, 54, 6, 398
 Kawakatu, N., Ohsuga, K. 2011, *MNRAS*, 417, 4, 2562–2570
 Kiuchi K., Shibata M., Montero P. J. Font J. A. 2011, *Physical Review Letters*, 106, 251102
 Komissarov S. S., 2006, *MNRAS*, 368, 993
 Kovar J., Slany P., Stuchlik Z., Karas V., Cremaschini C. & Miller J.C., 2011, *Phys. Rev. D*, 84, 084002
 Kozłowski M., Jaroszynski M., Abramowicz M. A., 1979, *A&A*, 63, 1–2, 209–220
 Krolik J. H. & Hawley J. F., 2002, *ApJ*, 573, 754
 Kucáková H., Slaný P. & Stuchlík Z., 2011, *JCAP*, 01, 033
 Lasota J.-P., Vieira R.S.S., Sadowski A., Narayan R. & Abramowicz M. A., 2016, *A&A*, 587, A13
 Lei Q., Abramowicz M. A., Fragile P. C., Horak J., Machida M. & Straub O., 2009, *A&A*, 498, 471
 Li, L. X. 2012, *MNRAS*, 424, 1461
 Lovelace R. V. E. & Chou T., 1996, *ApJ*, 468, L25
 Lyutikov M., 2009, *MNRAS*, 396, 3, 1545–1552
 Madau P., 1988., *ApJ*, 1, 327, 116–127
 Marchesi S. et al., 2016, *ApJ*, 830, 100
 Marchesi S., Ajello M., Comastri A., Cusumano G., Parola V. L. & Segreto A., 2017, *ApJ*, 836, 1 116
 Masini A. *et al.*, 2016, *A&A*, 589, A59
 Montero P. J., Zanotti O., Font J. A. & Rezzolla L., 2007, *MNRAS*, 378, 1101
 Nixon N., King A., Price D. & Frank J., 2012, *ApJ*, 757, L24
 Oka, T., Tsujimoto, S., Iwata, Y., Nomura, M. & Takekawa, S. 2017, *Nature Astronomy-Letter*, doi:10.1038/s41550-017-0224
 Paczyński B., 1980 *Acta Astron.*, 30, 4
 Paczyński B., 2000, *astro-ph/0004129*
 Parker E. N., 1955, *ApJ*, 122, 293
 Parker E. N., 1970 *ApJ*, 160, 383
 Porth O., Olivares H., Mizuno Y., et al., 2017, *Comput. Astro-&Cosm.*, 4, 1
 Pugliese D. & Kroon J. A. V., 2012, *Gen. Rel. Grav.*, 44, 2785
 Pugliese D. & Montani G., 2013, *EPL*, 101, 1, 19001
 Pugliese D., Montani G. & Bernardini M. G., 2013, *MNRAS*, 428, 2, 952
 Pugliese D. & Montani G., 2015, *Phys. Rev. D*, 91, 8, 083011
 Pugliese D., Quevedo H. & Ruffini R., 2011, *Phys. Rev. D*, 84, 044030
 Pugliese D., Quevedo H. & Ruffini R., 2013, *Phys. Rev. D*, 88, 024042
 Pugliese D. & Quevedo H., 2015, *Eur. Phys. J. C*, 75, 5, 234
 Pugliese D. & Stuchlik Z., 2015, *ApJS*, 221, 25
 Pugliese D. & Stuchlik Z., 2016, *ApJS*, 223, 2, 27
 Pugliese D. & Stuchlik Z., 2017a, *ApJS*, 229, 2 40
 Pugliese D. & Stuchlik Z., 2017b, submitted
 Pugliese D. & Stuchlik Z., 2017c *submitted*
 Pugliese D. & Stuchlik Z., 2018, *JHEAp*, 17, 1
 Reyes-Ruiz M., Stepinski T. F., 1999, *A&A*, 342, 892–900
 Ryu V., Schleicher D. R.G., Treumann R.A. et al., 2012 *Space Sci. Rev.*, 166, 1–35
 Sadowski A., Lasota J.P., Abramowicz M. A., & Narayan R., 2016, *MNRAS*, 456, 4, 3915
 Safarzadeh M., Naoz S., Sadowski A., Sironi L. & Narayan R., 2017, *arXiv:1701.03800*
 Siegel D. M., Ciofi R., Harte A. I. and Rezzolla L., 2013, *Phys. Rev. D*, 87, 12, 121302
 Schee J. & Stuchlik Z., 2009, *Gen. Rel. Grav.*, 41, 1795
 Schee J. & Stuchlik Z. 2013, *JCAP*, 1304, 005
 Sikora M., 1981, *MNRAS*, 196, 257
 Slany P., Kovar J., Stuchlik Z. & Karas V., 2013 *ApJS*, 205, 3
 Slaný & Stuchlík Z., 2005, *Class. Quantum Grav.*, 22, 2005, 3623
 Sochora V., Karas, Svoboda J., Dovciak M., 2011, *MNRAS*, 418, 276–283

- Storchi-Bergmann T., Schimoia J. S., Peterson B. M., et al., 2017, ApJ, 835, 236
- Stuchlik Z., 2005, Mod. Phys. Lett. A, 20, 561
- Stuchlik Z., Hledik S. & Truparova K., 2011, Class. Quant. Grav., 28, 155017
- Stuchlik Z. & Kovar J. 2008, Int. J. Mod. Phys. D, 17, 2089-105
- Stuchlik Z., Pugliese D., Schee J. & Kucáková H., 2015, Eur. Phys. J. C, 75, 9, 451
- Stuchlik Z., Slany P., Kovar J., 2009, Class. Quantum Grav., 26, 215013
- Stuchlik Z. & Schee J., 2010, Class. Quant. Grav., 27, 215017
- Stuchlik Z. & Schee J., 2013, Class. Quant. Grav., 30, 075012.
- Yoshizawa A., Itoh S. I., Itoh K., 2003, *Plasma & Fluid Turbulence: Theory and Modelling*, CRC Press
- Wielgus, M., Fragile, P. C., Wang, Z., & Wilson, J. 2015, MNRAS, 447, 359
- Volonteri, M., 2007, ApJ, 663, L5
- Volonteri, M., 2010, A&AR, 18, 279
- Volonteri M., Haardt F. & Madau P., 2003, ApJ, 582, 559
- Volonteri, M., Sikora, M., Lasota, J.-P., 2007, ApJ, 667, 704
- Zanotti O. & Pugliese D., 2015, Gen. Rel. Grav., 47, 4, 44

This paper has been typeset from a $\text{\TeX}/\text{\LaTeX}$ file prepared by the author.